GSC Advanced Research and Reviews
eISSN: 2582-4597 CODEN (USA): GARRC2
Cross Ref DOI: 10.30574/gscarr
Journal homepage: https://gsconlinepress.com/journals/gscarr/

(RESEARCH ARTICLE)

Check for updates

Synthesis, characterization and optical properties of $Na_{0.7}K_{0.3}Li_3SiO_4$ phosphor doped with Ce^{3+} and Dy^{3+}

Yogesh Bhojraj Wankhede * and Raju Madan Belekar

Department of Physics, Institute of Science, R.T Road, Civil Lines, Nagpur, Maharashtra, India- 440001.

GSC Advanced Research and Reviews, 2024, 19(01), 200-214

Publication history: Received on 05 March 2024; revised on 18 April 2024; accepted on 21 April 2024

Article DOI: https://doi.org/10.30574/gscarr.2024.19.1.0144

Abstract

$Na_{0.7}K_{0.3}Li_3SiO_4$ phosphors doped with Ce^{3+} and Dy^{3+} ions were synthesized in the present investigation using a microwave-assisted solution combustion synthesis method and subsequently underwent thermal treatment at 800°C. The synthesized material was analyzed using X-ray diffraction and scanning electron microscopy (SEM), while its photoluminescence properties were examined by excitation and emission spectroscopy at room temperature. X-ray diffraction (XRD) verified phase-pure orthorhombic crystal structures, characterized by space group $I4_1/a$ and a crystalline size of 55.56 nm, as determined by the Debye-Scherrer formula. SEM images revealed numerous approximately spherical irregular particles, with an average particle size of 45 nm. Photoluminescence (PL) investigations revealed blue emission in Ce^{3+}-doped materials associated with 5d → 4f transitions and distinctive yellow and blue emissions in Dy^{3+}-doped samples resulting from $^4F_{9/2} \rightarrow {}^6H_{11/2}$ transitions. The optical band gap was determined via UV-Vis spectroscopy and Tauc plots, yielding values of 4.93 eV for Ce^{3+}-doped samples and 5.13 eV for Dy^{3+}-doped samples. These phosphors demonstrate favourable luminescent characteristics for ultraviolet-excited white LED applications.

Keywords: Microwave-Assisted; Combustion; Photoluminescence; White LED

1. Introduction

Rare-earth (RE)-doped phosphor systems have drawn considerable attention owing to their widespread applications in display devices, lamp phosphors, and white light production [1–3](Reddy, 2023). These materials, when excited by a suitable wavelength, demonstrate a high luminescence yield and can be modified to enhance chromaticity. These are possible choices for luminescent materials designed for flat displays, mercury-free fluorescent lights, plasma display panels, X-ray tubes, and numerous detection systems. The observed photoluminescence (PL) in these materials is attributed to the f–f or f–d transitions of rare-earth ions, with intensity depending on site symmetry and ligand properties. Recently, several groups have reported various RE-doped phosphors demonstrating efficient and narrow emissions within the visible spectrum. Various borates (e.g., YBO_3 and $YAl_3B_4O_{12}$) and phosphates (including pyrophosphates and borophosphates) are recognized as highly effective host matrices [4–5](Mayavan et al., 2024; Ugemuge et al., 2021). Moreover, silicate-based host lattices have been proposed to enhance the luminescence from rare-earth ions.

The phosphor activated by Eu^{2+} has been recognized as an outstanding yellow phosphor ideal for light-emitting diode (LED)-based solid-state lighting applications (Gupta et al., 2012; Yan et al., 2021). Zinc silicate doped with Mn^{2+}, Eu^{3+}, Tb^{3+}, Dy^{3+}, and Ce^{3+} has been extensively described for its luminous characteristics [9–13](Akhnazarova et al., 2011; Matsuzawa et al., 1996; Saito, 2004). The tetrahedral silicate $(SiO_4)^{2-}$ ion provides significant mechanical strength and stability to the phosphor in these matrices. The photoluminescence investigations of lithium titanate, tantalate, niobate,

* Corresponding author: Yogesh Bhojraj Wankhede.

aluminate, and tetraborate compounds are comprehensively detailed (Huang et al., 2024; Kakde et al., 2023; B. Wang et al., 2018; F. Wang et al., 2017; Wani et al., 2022). Moriyama and his associates have recorded the in situ luminescence investigations of defect centers produced in ortho and meta lithium silicates exposed to proton beam irradiation (Varma et al., 2016).

Phosphor materials doped with rare earth ions have received significant attention for lighting and optoelectronic applications because of their high quantum efficiency, chemical stability, and unique emission lines.

Luminescence in these advanced materials arises from 5d to 4f transitions in rare earth ions inside appropriate host materials. These ions absorb energy and re-emit it as brilliant light. Among the various host materials, **silicate-based phosphors** have emerged as interesting host materials due to their thermal stability, broad bandgap, and highly adaptable crystal structures.

Our research focuses on a mixed alkali silicate host: $\mathbf{Na_{0.7}K_{0.3}Li_3SiO_4}$. This compound provides a stable orthorhombic structure (as shown in Figure 1), making it an ideal, flexible framework to accommodate, or "trap," dopant ions like Cerium (Ce) and Dysprosium. Ce3+ displays extensive blue emission resulting from 5d-4f transition, and Dy3+ shows narrow emission in the blue and yellow spectra for white light production.

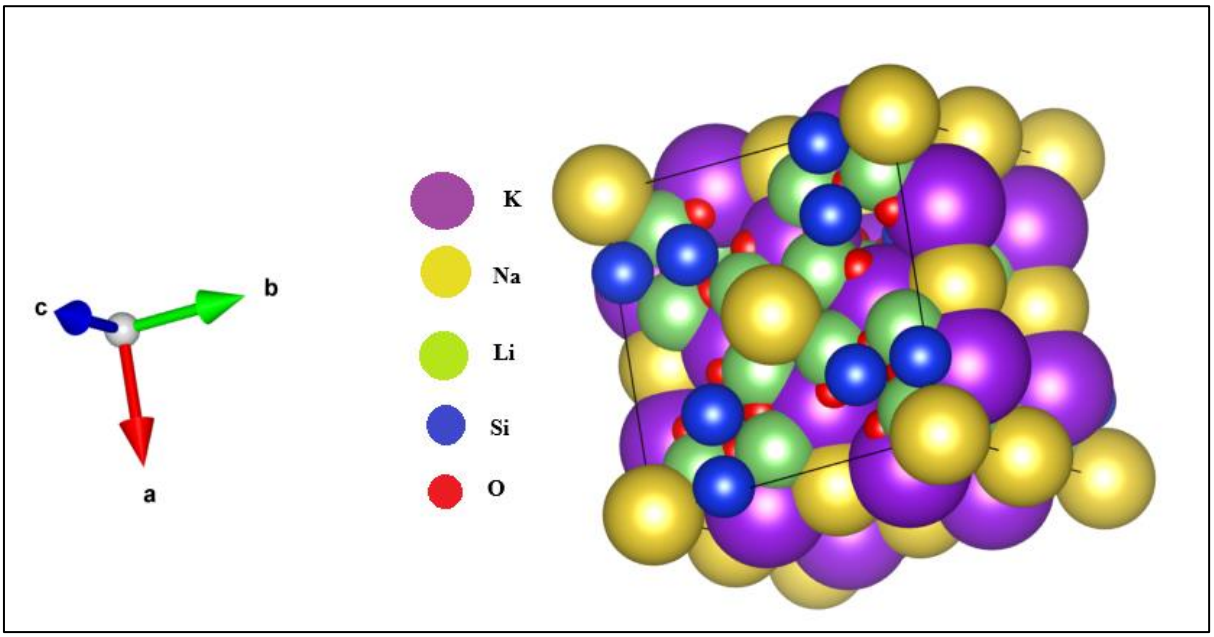

Figure 1 Crystal structure of $Na_xK_{1-x}Li_3SiO_4$

2. Materials and Methods

The materials were synthesized by microwave-assisted solution combustion synthesis method. This technique involves an exothermic redox reaction between an oxidizer and a fuel within an aqueous solution, leading to the formation of fine, homogeneous powders with controlled stoichiometry and morphology [12] (Wani et al., 2022).

2.1. Materials required

Lithium Nitrate ($LiNO_3$), Sodium Nitrate ($NaNO_3$), Potassium Nitrate (KNO_3), Silicic Acid (H_4SiO_4), Dysprosium Oxide (Dy_2O_3), Cerium nitrate $Ce(NO_3)_3$, Urea $CO((NH_2)^2$ and Distilled water.

Synthesis : First Dissolve stoichiometric quantities as per table 1 of $LiNO_3$, $NaNO_3$, and KNO_3 in distilled water to produce a clear solution, designated as Mixture 1. Next incorporate silicic acid (H_4SiO_4) and the calculated quantities of $Ce(NO_3)_3$ or Dy_2O_3,while maintaining continuous stirring, which is referred to as Mixture 2. Take proper quantity of urea and dissolve it into Mixture 1, for combustion. Carefully combine, Mixture 2 into Mixture 1, and provide heat using a heating mantle. The liquid dehydrates and experiences self-sustained combustion, resulting in a foamy product. Now, transfer the foamy product to a preheated microwave oven for a duration of 5 minutes to initiate the combustion

process. After the combustion process, allow the substance to reach room temperature, and then pulverize it into a fine powder. At last, sinter the powder at 800°C for four hours to improve crystallinity and phase purity. Now, grind the sintered powder for characterization.

Table 1 List of material synthesised

Sample No.	Materials	List of dopants
1.	$Na_{0.7}K_{0.3}Li_3SiO_4$	1. Dy^{3+} (3mol %) 2. Dy^{3+} (5mol %) 3. Dy^{3+} (7mol %)
2.	$Na_{0.7}K_{0.3}Li_3SiO_4$	1. Ce^{3+} (3mol %) 2. Ce^{3+} (5mol %) 3. Ce^{3+} (7mol %)

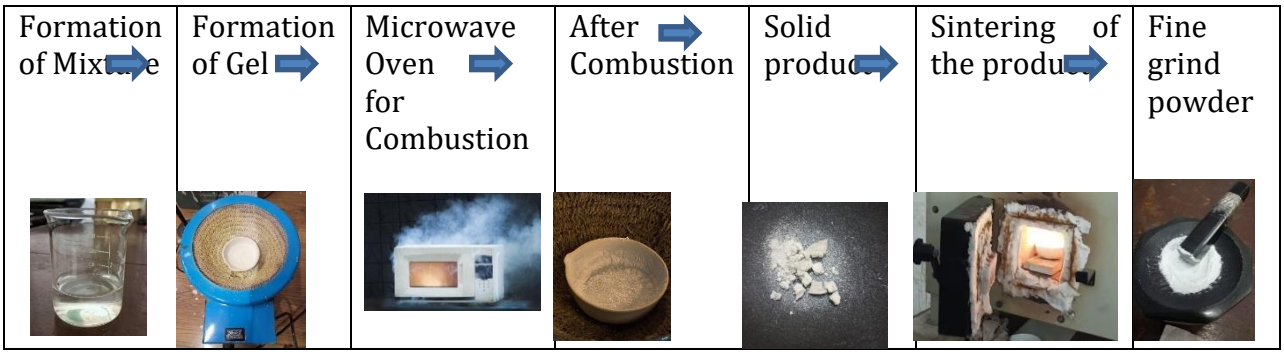

Figure 2 Steps involved during synthesis of material

3. Results and Discussion

3.1. X-Ray Diffraction (XRD) Analysis

The X-ray Diffraction (XRD) method is one of the analytical tools to study the crystallographic structure, phases, and structural parameters of materials. When the X-rays are exposed to a crystalline substance, they are diffracted from the atomic planes of the material. Based on the diffraction data, it is possible to obtain information about the interatomic plane distances using Bragg's equation [13-14] (Kakde et al., 2023; Wang et al., 2017):

$n\lambda = 2d \sin\theta$ ---------- (1)

$d = n\lambda / (2 \sin\theta)$ --------- (2)

Where:

n – order of reflection (for first-order diffraction, the parameter n = 1);

λ – wavelength of the X-rays;

d – interplanar distance (distance between atomic planes in the crystal).

3.2. Estimation of Crystallite Size

The XRD line broadening is analysed using the Scherrer equation to determine the size of the crystalline phase domains (crystallites):

$$D = (K\lambda) / (\beta \cos \theta) \text{ ---------- (3)}$$

Where:
D – average crystallite size;
K – shape factor (K ≈ 0.9);
λ – X-ray wavelength (1.5406 Å);
β – full width at half maximum (FWHM) of the line (in radians);

θ – Bragg angle.

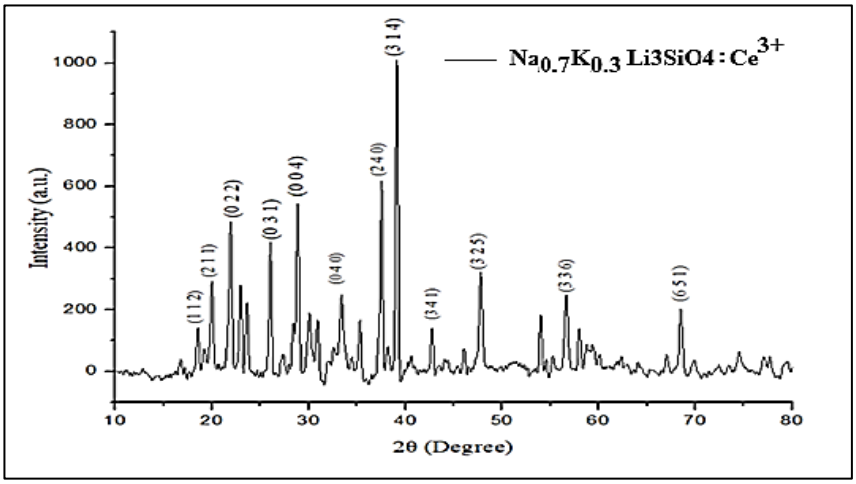

Figure 3 XRD analysis of **Ce^{3+}doped** $Na_{0.7}K_{0.3}Li_3SiO_4$

XRD analysis of the synthesized Ce^{3+}-doped $Na_{0.7}K_{0.3}Li_3SiO_4$ nanocomposites fabricated by combustion synthesis is depicted in Fig. 3. All peaks detected in the sample correspond to the standard data for the orthorhombic structure of $Na_{0.7}K_{0.3}Li_3SiO_4$ (1518159.cif). The studied system is also characterized by an orthorhombic structure with an end-centered unit cell (space group $I4_1/a$). A significant shift in the positions of the XRD peaks indicates changes in the crystal structure of the synthesized nanocomposite. This phenomenon results from the introduction of Ce^{3+} ions into the structure of the compound. In particular, the ionic radius of the Ce^{3+} ion is much larger than that of the alkali metal ions, Na^+ and Li^+. Thus, when Ce^{3+} replaces these ions, changes occur in the lattice parameters.

Table 2 Calculation of d (interplanar distance) and D (crystallite size) in Ce^{3+}-doped $Na_{0.7}K_{0.3}Li_3SiO_4$

2θ degrees	Intensity a.u.	β radians	θ degrees	d Å	D Å	(h k l)
18.48	477	2.08547	9.24	4.797275717	38.59430253	1 1 2
20	663	0.30771	10	4.435980903	262.1573064	2 1 1
21.96	926	0.3547	10.98	4.044284336	228.1486117	0 2 2
26.04	881	0.27387	13.02	3.419131049	297.7293626	0 3 1
28.88	1056	0.33713	14.44	3.089033479	243.3316944	0 0 4
33.4	783	0.63697	16.7	2.680604839	130.2120045	0 4 0
37.56	1154	0.27218	18.78	2.392717298	308.289084	2 4 0

39.12	1496	0.27163	19.56	2.300819137	310.3788134	3 1 4
42.76	441	82.9751	21.38	2.113005832	1.028187107	3 4 1
47.8	600	0.35871	23.9	1.901310616	242.2393562	3 2 5
56.64	511	0.00305	28.32	1.623750562	29588.20826	3 3 6
68.48	431	0.337	34.24	1.369031222	285.1566602	6 5 1

In order to evaluate the structural properties of the Ce^{3+}-doped lithium silicate, two important values were determined using the X-ray diffraction (XRD) results. The average interplanar spacing (d) was determined to be 1.1969 Å for the Ce^{3+}-doped lithium silicate, which represents the distance between two adjacent planes. The average value of crystallite size (D) for the Ce^{3+}-doped sample was 2903.22 Å (290 nm), showing a relatively large crystallite size.

The results of X-ray diffraction (XRD) of the Dy^{3+}-doped $Na_{0.7}K_{0.3}Li_3SiO_4$ material, prepared by the combustion method, are depicted in Figure 4. The peak positions obtained from the experiment match well with those of orthorhombic $Na_{0.7}K_{0.3}Li_3SiO_4$ (CIF file 1518159). Diffraction analysis revealed that the Dy^{3+}-doped sample consists of orthorhombic crystal structure with an end-centered lattice, which belongs to the space group $I4_1/a$.

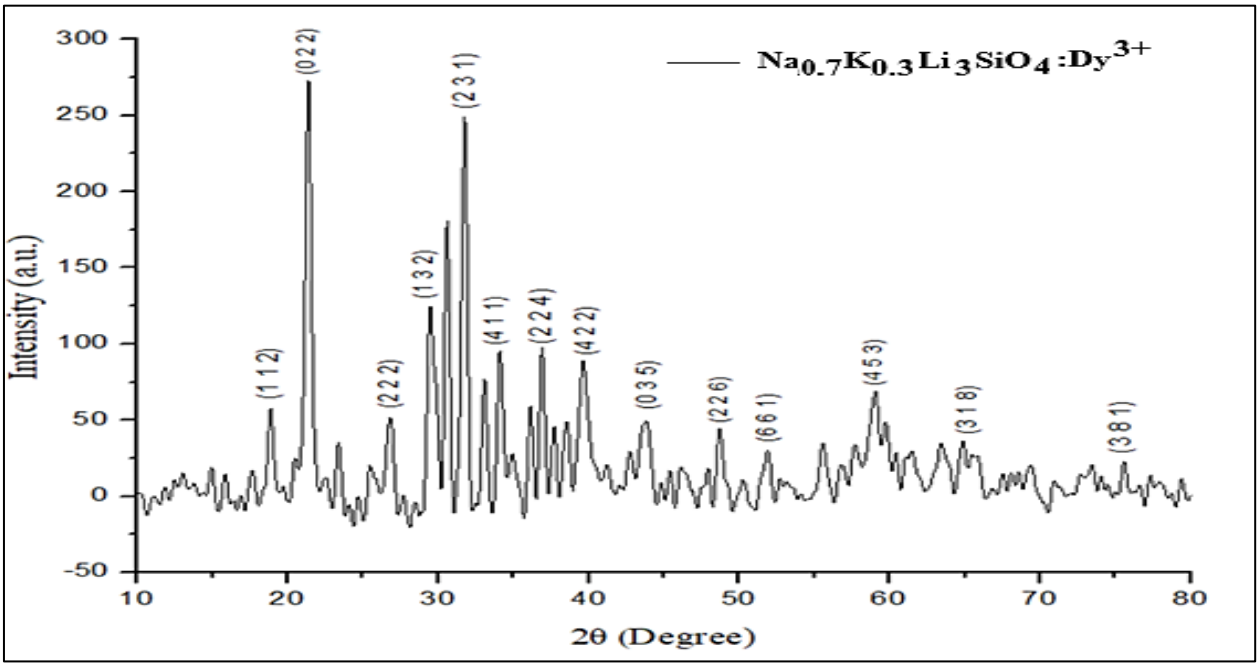

Figure 4 XRD patterns of the doped Dy^{3+} in $Na_{0.7}K_{0.3}Li_3SiO_4$

The XRD pattern of Dy^{3+}-doped $Na_{0.7}K_{0.3}Li_3SiO_4$ for the current sample is presented in figure 4. The presence of clear and sharp diffraction peaks indicates the crystallinity of the prepared sample. All the main peaks represent the orthorhombic phase of $Na_{0.7}K_{0.3}Li_3SiO_4$, and there are no other peaks observed. Hence, it can be confirmed that Dy^{3+} ions have been successfully doped in the host lattice. Although Dy^{3+} ions have been doped in the host lattice, the orthorhombic phase has remained unchanged, revealing that the host lattice is capable of accommodating rare earth ions. There could be small changes in the intensity and position of the peaks due to lattice strain or differences in ionic radii.

Table 3 Calculation of d (interplanar distance) and D (crystallite size) in Dy^{3+}-doped $Na_{0.7}K_{0.3}Li_3SiO_4$

2θ degrees	Intensity a.u	β radians	θ degrees	d Å	D Å	(h k l)
18.88	573	16.2584	9.44	4.696530832	4.953212083	1 1 2
21.36	967	0.46385	10.68	4.156513087	174.2875807	0 2 2
26.8	776	0.93532	13.4	3.323870414	87.31362546	2 2 2
29.48	921	1.69358	14.74	3.027514146	48.50452596	1 3 2
31.76	1090	0.42354	15.88	2.815182269	195.0110306	2 3 1
34.12	849	2.1725	17.06	2.625667807	38.25059886	4 1 1
36.92	695	1.9185	18.46	2.432711783	43.65513325	2 2 4
39.64	652	1.66365	19.82	2.271826879	50.7590035	4 2 2
43.84	543	4.13755	21.92	2.063423494	20.69671479	0 3 5
48.68	539	1.6746	24.34	1.868977302	52.06793908	2 2 6
51.88	473	13.9558	25.94	1.76096871	6.330271305	6 6 1
59.08	469	2.72352	29.54	1.562376203	33.52736093	4 5 3
64.88	454	5.50402	32.44	1.436012037	17.10237561	3 1 8
75.56	368	18.6215	37.78	1.25736332	5.397620708	3 8 1

The d-spacing value obtained was 2.5213 Å, representing the spacing between atomic planes in the crystal. Any deviation from the undoped sample's d-spacing suggests lattice distortion due to the presence of Dy^{3+} ions. The average crystallite size of the Dy^{3+}-doped $Na_{0.7}K_{0.3}Li_3SiO_4$ was about 55.56 nm.

Both the Ce^{3+} and Dy^{3+} doped samples showed well-defined peaks attributed to the orthorhombic structure (COD No. 1518159). The peak shifts in the Ce^{3+} doped sample were a result of lattice strain because of ionic size differences and had an average crystallite size of about 290 nm. The Dy^{3+} doped sample maintained its phase purity and had small crystallite sizes (~55 nm).

3.3. Morphological Analysis

The SEM micrographs of the host $Na_{0.7}K_{0.3}Li_3SiO_4$ phosphor at a sintering temperature of 900°C are shown in fig. 5. The SEM micrographs in Figure 5 show the agglomerated structure of particles from the prepared samples, with an average diameter of 10 μm, resulting from the quenching of phosphate samples at relatively lower temperatures.

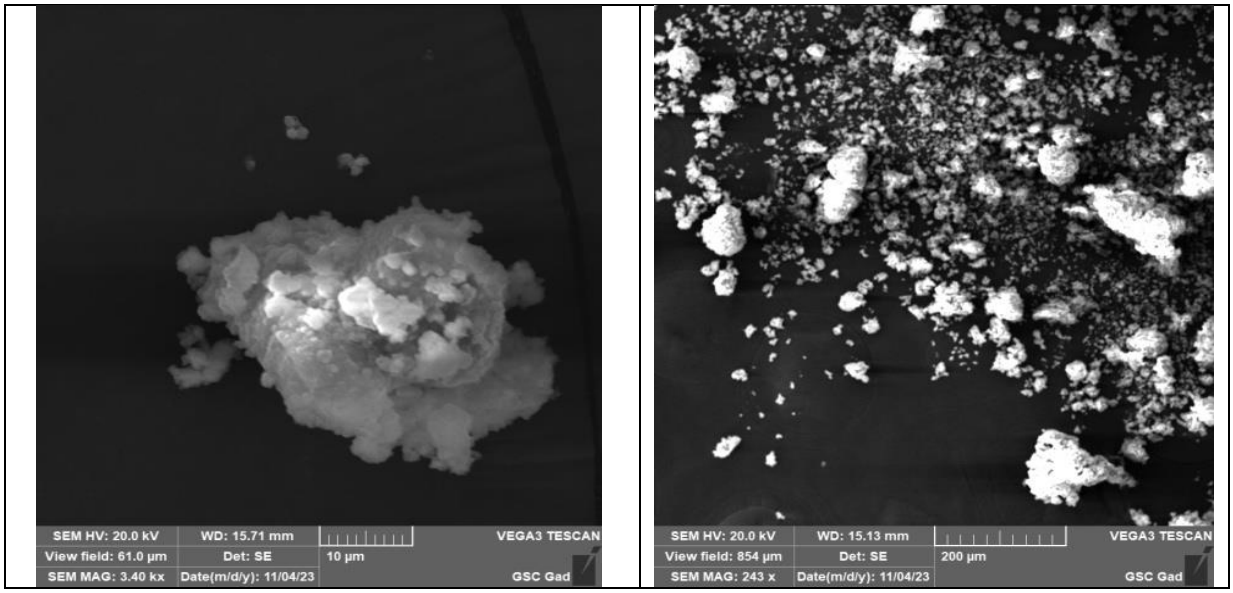

Figure 5 SEM micrographs of host $Na_{0.7}K_{0.3}Li_3SiO_4$ phosphor

3.4. FTIR (Fourier Transform Infrared Spectroscopy)

Fourier Transform Infrared (FTIR) spectroscopy is a spectroscopic technique that uses a Fourier transform infrared spectrometer to acquire an infrared spectrum of the absorption or emission of a substance. According to FTIR spectroscopy, molecules absorb energy at characteristic frequencies that correspond to the vibrational modes of bonding. An FTIR spectrometer passes an IR light through a sample, and detects the wavelengths of light either emitted or absorbed by the substance.

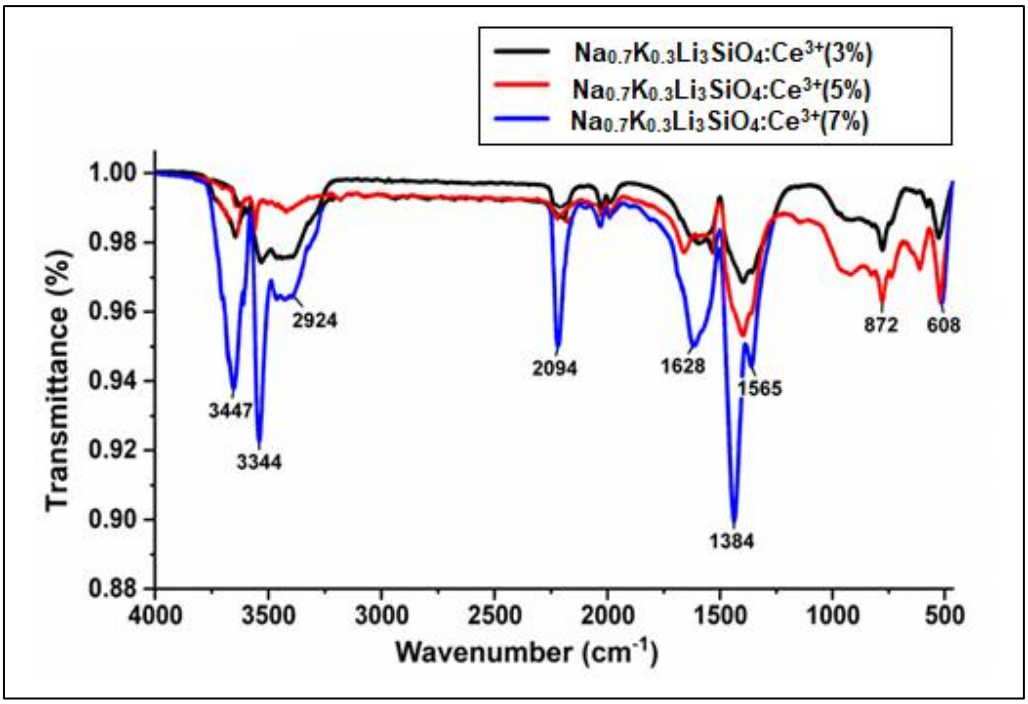

Figure 6 (a) Fourier transform infrared (FTIR) spectrum of Ce^{3+} doped $Na_{0.7}K_{0.3}Li_3SiO_4$ sample

FTIR is an analytical technique used to identify and characterize materials based on their molecular fingerprint. This type of spectroscopy enables one to obtain information regarding molecular composition and structure through infrared absorption analysis. Different bonds have unique vibrational energies that correspond to their infrared

absorption frequencies. Thus, FTIR analysis can be employed to identify the functional groups present, types of bonds formed, and molecular structures in a sample.

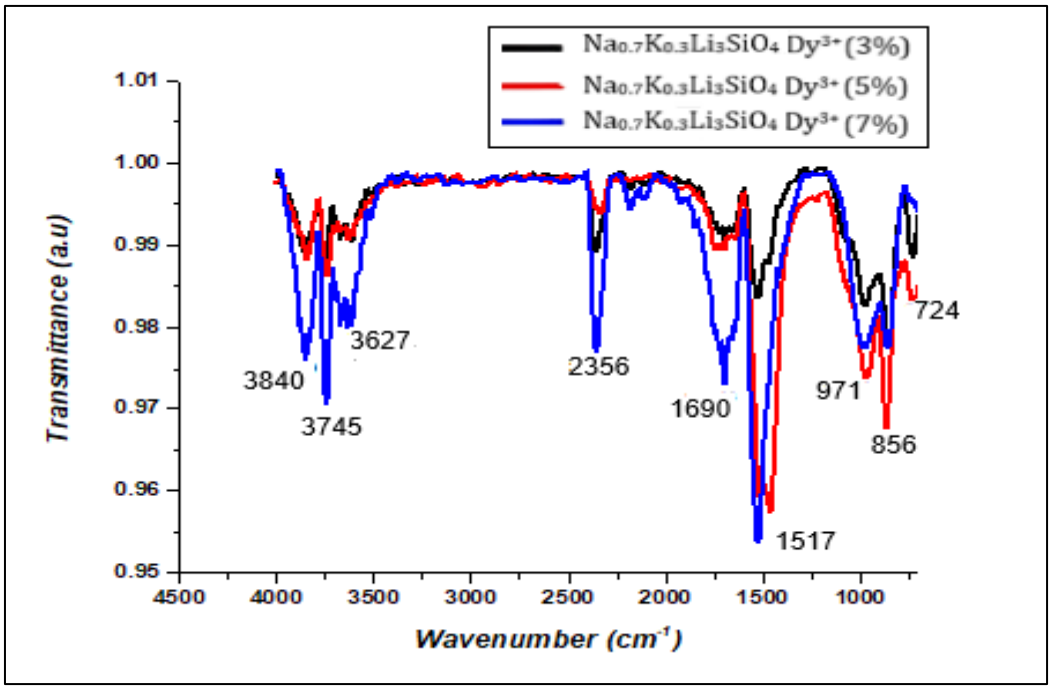

Figure 6 (b) Fourier transform infrared (FTIR) spectrum of Dy^{3+} doped $Na_{0.7}K_{0.3}Li_3SiO_4$ sample

Table 4 FTIR Assignment Table Ce3+ doped $Na_{0.7}K_{0.3}Li_3SiO_4$ sample.

Wavenumber (cm-1)	Functional Group	Vibration type
$Na_{0.7}K_{0.3}Li_3SiO_4:Ce^{3+}$(3%)		
614.91	C-Br	Stretching
656.33	C-Br	Stretching
732.37	C-H	Bending
856.14	Si-O	Stretching
$Na_{0.7}K_{0.3}Li_3SiO_4:Ce^{3+}$(5%)		
652.26	C-Br	Stretching
687.71	C-Br	Stretching
809.57	C-Cl	Stretching
860.59	C-Cl	Bending
928.20	C-H	Bending
$Na_{0.7}K_{0.3}Li_3SiO_4:Ce^{3+}$(7%)		
623.21	C-Br	Stretching
645.08	C-Cl	Stretching
664.29	C-Cl	Stretching
858.37	Si-O	Stretching

Table 5 FTIR Assignment Table Dy^{3+} doped $Na_{0.7}K_{0.3}Li_3SiO_4$ sample

$Na_xK_{1-x}Li_3SiO_4:Dy^{3+}$(3%)		
Wavenumber (cm-1)	Functional Group	Vibration type
1463.24	CH_2 / CH_3	Bending
1514.79	C=C	Stretching
1530.54	NO_2	Stretching
1647.94	C=O	Stretching
1690.89	C=O	Stretching
1706.64	C=O	Stretching
1742.43	C=O	Stretching
$Na_{0.7}K_{0.3}Li_3SiO_4:Dy^{3+}$(5%)		
1464.68	CH_2 / CH_3	Bending
1509.06	C=C	Stretching
1645.08	C=O	Stretching
1692.32	C=O	Stretching
1741	C=O	Stretching
1799.70	C=O	Stretching
$Na_{0.7}K_{0.3}Li_3SiO_4:Dy^{3+}$(7%)		
1426.02	COO^-	Stretching
1464.68	CH_2 / CH_3	Bending
1514.79	C=C	Stretching
1530.30	NO_2	Stretching
1546.85	C=O	Stretching
1646.51	C=O	Stretching
1690.89	C=O	Stretching
1743.87	C=O	Stretching

The FTIR spectra of Ce^{3+} and Dy^{3+} doped $Na_{0.7}K_{0.3}Li_3SiO_4$ phosphors are shown in figures 6 (a) and 6(b), which confirm the formation of a stable silicate network, with characteristic Si–O–Si stretching and bending vibrations observed between 600–1100 cm^{-1}. Ce^{3+} doped samples show peaks at 614–928 cm^{-1}, indicating minor lattice distortions due to Ce^{3+} incorporation. Dy^{3+} doped samples exhibit additional peaks between 500–900 cm^{-1}, attributed to Dy–O stretching, suggesting successful Dy^{3+} substitution. These spectral changes confirm effective doping and structural integrity, essential for optimizing luminescent properties.

3.5. UV-Visible Spectroscopy

UV-visible spectroscopy is one of the most commonly employed spectroscopic techniques for studying the electronic transitions within substances based on the measurement of either the absorbance or the transmission of ultraviolet and visible radiation. It is based on the concept that when UV-Vis light passes through a substance, different wavelengths will be absorbed due to the specific electronic configuration of the substance [18]. This technique is useful in determining the optical band gap and the electronic behavior of the doped and undoped phosphors. The present investigation involves the analysis of the optical band gap of $Na_{0.7}K_{0.3}Li_3SiO_4$ phosphors doped with Ce^{3+} and Dy^{3+} by performing UV-Visible diffuse reflectance spectroscopy (DRS) studies on the synthesized phosphors to study their

optical properties. The optical band gap of the samples was determined using Tauc's relation [18] (Gupta et al., 2021), which correlates the absorption coefficient (α) with the photon energy (hν) through the following relationship:

$$(\alpha h\nu)n = A\,(h\nu - Eg) \quad (4)$$

where A is the proportionality constant, Eg is the optical band gap, and n is related to the type of electronic transitions, which can be equal to ½ for allowed direct transitions and 2 for allowed indirect transitions.

For the current analysis, the Tauc plot was constructed by plotting $(\alpha h\nu)^2$ versus hν to evaluate the indirect allowed band gap. The band gap value is obtained by extrapolating the linear portion of the curve to the photon energy axis where $(\alpha h\nu)^2 = 0$.

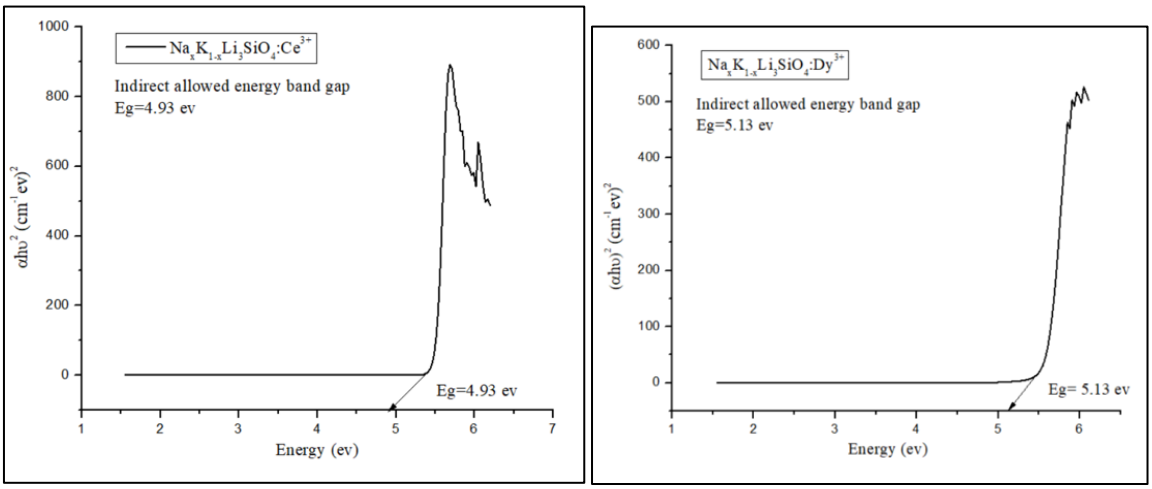

Figure 7 The plots of $(\alpha h\nu)^2$ as a function of photon energy

The diffuse reflectance spectra of all samples exhibited a prominent absorption edge around 355 nm, indicating strong UV absorption. The Tauc plots for Ce^{3+} and Dy^{3+} doped samples are shown in Figure 7. Optical gaps (Figure 7) obtained from the analysis of the graph reveal the indirect allowed energy of about 4.93 eV and 5.13 eV for samples doped with Ce^{3+} and Dy^{3+} ions, respectively. These data demonstrate the effect of rare-earth dopants on the electronic structure of the host material due to the creation of localized states associated with the presence of dopant ions. The larger bandgap of Dy^{3+} samples compared to Ce^{3+} ones can be explained by the greater impact on the lattice or other features related to the electronic configuration. This indicates the possibility of using rare-earth doping to control optical characteristics, making silicate phosphors suitable for UV-activated luminescent devices.

3.6. Photoluminescence Study

Properties of rare earth ions doped in $Na_{0.7}K_{0.3}Li_3SiO_4$ host matrices were studied via PL spectroscopy. Excitation and emission spectra of both Ce^{3+} and Dy^{3+} doped materials were obtained.

Ce^{3+}-Doped Samples: Figures 8(a), 8(b), and 8(c) show the excitation and emission spectra of the Ce^{3+}-doped samples. The effect of different Ce^{3+} doping concentrations (3%, 5%, and 7%) on PL characteristics of Ce^{3+}-doped $Na_{0.7}K_{0.3}Li_3SiO_4$ phosphors is discussed in this part of the experiment. In the excitation spectra of Ce^{3+} doped phosphors, the broad band is located at 250–360 nm due to the 4f → 5d allowed transition energy of Ce^{3+} ions [19]. (Wang et al., 2019)

For 3% Ce^{3+} doped phosphor sample, the excitation peak occurred at around 397 nm while the emission spectrum gave rise to a wide emission center at 471 nm that belongs to the 5d → 4f transition of Ce^{3+} ions causing blue emission. For 5% Ce^{3+} doped phosphors, there was no change in the position of excitation peak while the emission peak showed blueshift at 438 nm indicating increased crystal field effect.

For the phosphor at a concentration of 7%, a notable change in the excitation wavelength towards 253 nm occurred while its emission peak was centered around 470 nm. This implies considerable changes in crystal field environments because of either concentration quenching or the formation of Ce^{3+} clusters, resulting in energy-level variations.

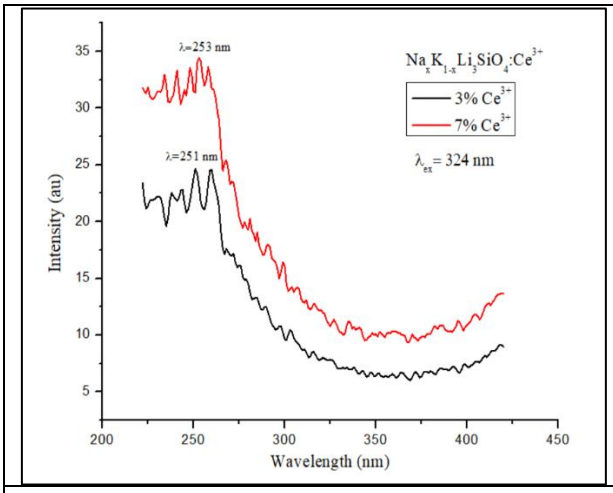

Figure 8(a) Excitation Spectra of $Na_{0.7}K_{0.3}Li_3SiO_4$: Ce^{3+} (3% and 7%) phosphors

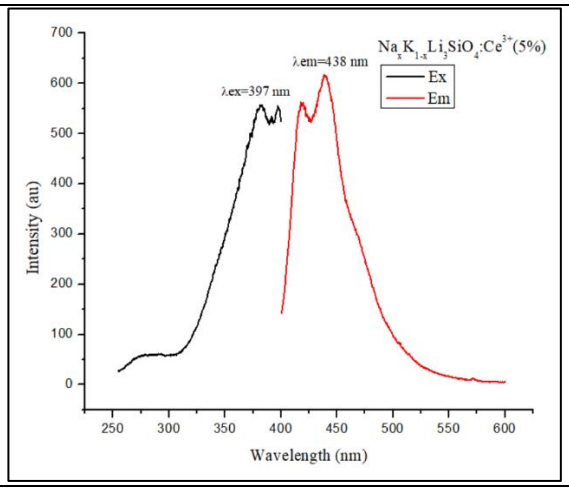

Figure 8(b) Excitation and emission spectra of $Na_{0.7}K_{0.3}Li_3SiO_4$: Ce^{3+}(5%) phosphors

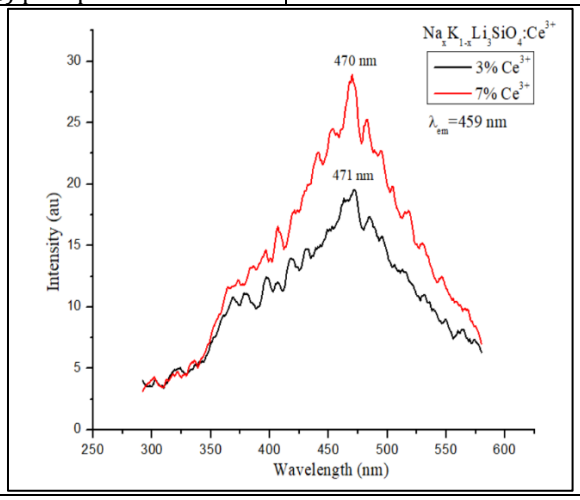

Figure 8(c) Emission spectra of $Na_{0.7}K_{0.3}Li_3SiO_4$: Ce^{3+} (3% and 7%)

Excitation and emission peaks in Ce^{3+}-doped $Na_{0.7}K_{0.3}Li_3SiO_4$ phosphors ranged from 253 nm to 397 nm and from 438 nm to 471 nm, respectively. On average, the excitation and emission peaks had 324 nm and 459 nm, respectively, which is typical for the Ce^{3+} 5d → 4f transitions. The sharp excitation spectrum was caused by 4f → 5d transitions. Shift of emission peaks from 471 nm to 438 nm indicated crystal field effects.

3.7. Dy^{3+}-Doped Samples:

Characteristic sharp excitation peaks caused by f–f transitions in Dy^{3+} doped samples exhibited a maximum at ~352 nm. Dy^{3+} emission spectra had two main peaks at ~480 nm (blue emission) and ~572 nm (yellow emission). These emissions corresponded to transitions from $4F_9/_2 \rightarrow 6H_{15}/_2$ and $4F_9/_2 \rightarrow 6H_{13}/_2$ states, respectively [5].

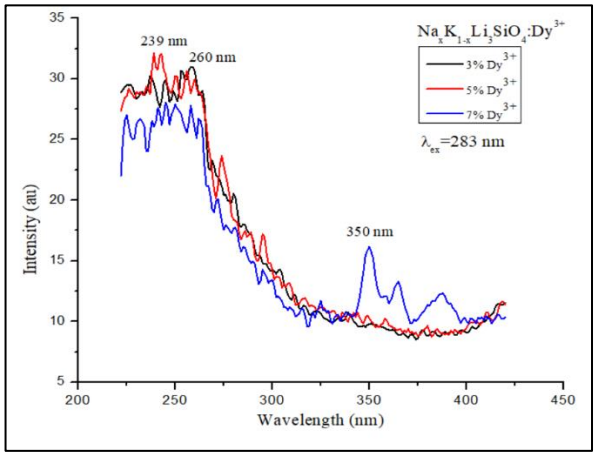

Figure 9(a) *Excitation spectra of* $Na_{0.7}K_{0.3}Li_3SiO_4$: Dy^{3+} (3%, 5%, 7%) phosphors

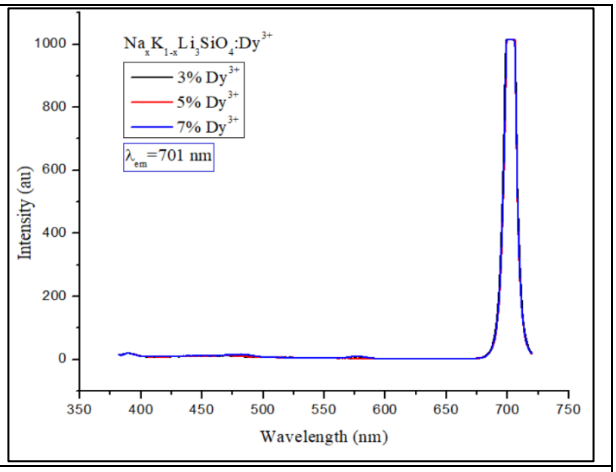

Figure 9(b) *Emission spectra of* $Na_{0.7}K_{0.3}Li_3SiO_4$: Dy^{3+} (3%, 5%, 7%) phosphors

The photoluminescent property of Dy^{3+}-doped $Na_{0.7}K_{0.3}Li_3SiO_4$ is demonstrated in Fig. 9(a) and Fig. 9(b). The PL properties are affected when the dopant concentration is altered in Dy^{3+}-doped $Na_{0.7}K_{0.3}Li_3SiO_4$ phosphors. As a result, excitation peaks were observed at approximately 260 nm, 293 nm, and 350 nm for doping concentrations of 3%, 5%, and 7%, respectively. However, the emission peaks were always found at 701 nm, even though the excitation wavelength was different, which corresponds to the $4F_9/_2 \rightarrow 6H_{11}/_2$ energy transition of the Dy^{3+} ion. This indicates that this phosphor may be used in optical communication and bio-imaging due to its near-infrared emission. An emission peak was observed at 701 nm, and two smaller peaks were noted at 480 and 572 nm, associated with the $^4F_9/_2 \rightarrow {}^6H_{15}/_2$ and $^4F_9/_2 \rightarrow {}^6H_{13}/_2$ transitions.

Finally, it can be concluded that Ce^{3+}-doped $Na_{0.7}K_{0.3}Li_3SiO_4$ phosphors show adjustable emission properties and are appropriate for the production of white LEDs and optoelectronics. Additionally, the yellow to blue emission intensity ratio (Y/B) depends on the asymmetry of sites surrounding Dy^{3+} ions.In conclusion, Ce^{3+}-doped $Na_{0.7}K_{0.3}Li_3SiO_4$ phosphors exhibit tuneable emission properties, making them ideal for white LED and optoelectronic applications. The yellow-to-blue emission intensity ratio (Y/B) is influenced by the local site symmetry around Dy^{3+} ions, with higher Y/B ratios indicating more asymmetric environments and enhanced yellow emission. This tunability offers potential for precisely controlling emission characteristics, crucial for efficient white light-emitting applications.

3.8. CIE Graph

The CIE 1931 chromaticity graph displays all the colors that can be perceived by the human eye. The graph plots colors according to two attributes: hue (color type) and saturation (intensity or color purity), which are collectively termed "chromaticity." It plays a vital role in understanding the color properties of different substances.

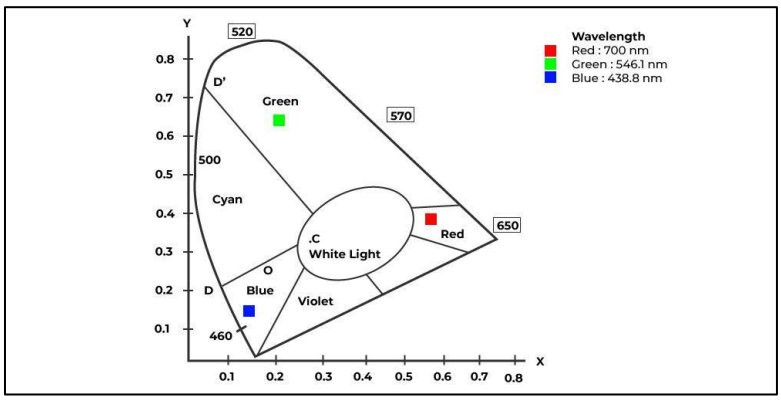

Figure 10 CIE chromacity diagram 1931

The CIE 1931 chromaticity graph depicts all visible colors from the human perspective. The graph plots spectral colors on a horseshoe-shaped curve (380–700 nm) and non-spectral purples on a straight line. The saturated colors lie on the edge, while the less saturated colors lie closer to the white point in the center.The diagram is defined by primary colours—red (700 nm), green (546.1 nm), and blue (435.8 nm)—which form a triangle enclosing all mixable colours. Each colour is identified by chromaticity coordinates (x, y), making the diagram useful for analysing and reproducing colours in materials and display technologies.

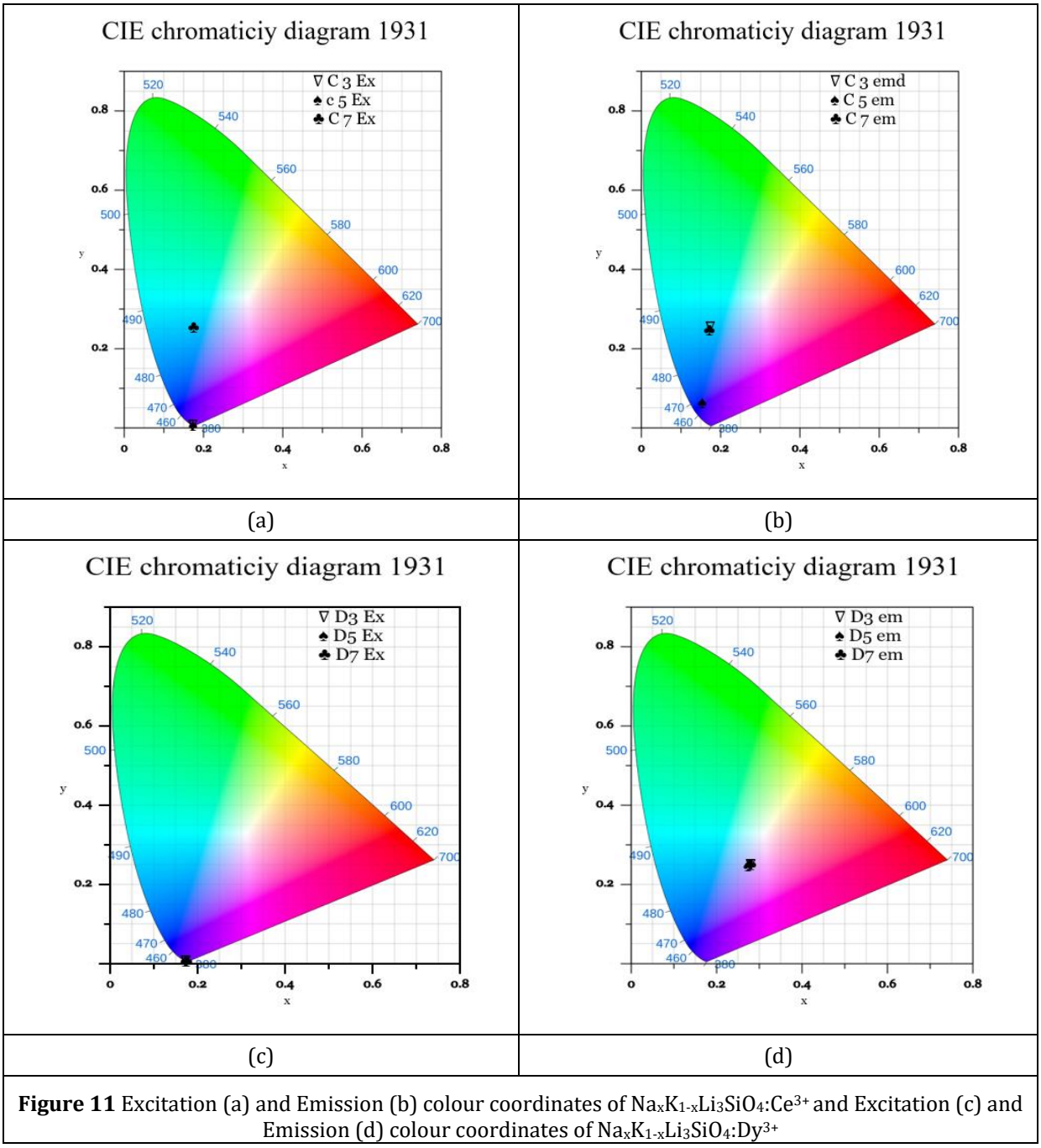

Figure 11 Excitation (a) and Emission (b) colour coordinates of $Na_xK_{1-x}Li_3SiO_4:Ce^{3+}$ and Excitation (c) and Emission (d) colour coordinates of $Na_xK_{1-x}Li_3SiO_4:Dy^{3+}$

The CIE coordinates of the Ce^{3+}-doped host are x=0.173 and y=0.087 for excitation (Fig. 11(a,b)), and x=0.165 and y=0.187 for emission.

The CIE coordinate of the Dy^{3+}-doped host for excitation (Fig. 11(c, d)) is found to be x=0.172 and y=0.005; for emission, x=0.277 and y=0.247.

The coordinates show that the phosphors have tunable colors, which imply a promising application for white LEDs.

4. Conclusion

The synthesis of Ce^{3+} and Dy^{3+}-doped $Na_{0.7}K_{0.3}Li_3SiO_4$ phosphors by the combustion method has been successfully achieved. The phosphors have been characterized by XRD, photoluminescence, FTIR, and UV-visible spectra.According to XRD, the samples doped with Ce^{3+} and Dy^{3+} retained their orthorhombic crystal structures with high crystallinity. The doping with Ce^{3+} caused a peak shift due to lattice distortion as a result of the difference in the sizes of the ions used. The samples showed a higher crystallite size of 290 nm and lower interplanar spacing of 1.1969 Å. The Dy^{3+}-doped samples produced sharp peaks without any second phases, with a crystallite size of 55.56 nm and an interplanar spacing of 2.5213 Å.Dy^{3+}-doped samples displayed characteristic f–f transitions, showing dual emissions around 480 nm and 572 nm. Additionally, a consistent near-infrared emission (~701 nm) at higher concentrations makes them promising for optoelectronic and bio-imaging applications. FTIR spectra confirmed the formation of a stable silicate network in both Ce^{3+} and Dy^{3+}-doped samples. The introduction of Ce^{3+} resulted in slight lattice distortions, but the inclusion of Dy^{3+} resulted in more peaks attributed to C–O stretching, which demonstrated doping success and some interactions without affecting the structure. The diffuse reflectance analysis, and Tauc plots showed that the optical band gap was modified from 4.93 eV for Ce^{3+} doped samples and 5.13 eV for Dy^{3+} doped samples. This shows a change in the electronic structure due to doping with rare-earth ions, thus showing the potential to tune the optical properties for various luminescent applications. $Na_{0.7}K_{0.3}Li_3SiO_4$ phosphors doped with Ce^{3+} and Dy^{3+} were successfully synthesized using a combustion method. Structural analysis confirmed orthorhombic phase retention and effective dopant substitution. Ce^{3+} doped samples exhibited tuneable blue emissions, while Dy^{3+} doped samples showed characteristic f–f emissions. The optical band gap was found to be tuneable based on dopant type. These results establish the material as a promising candidate for UV-excited white light-emitting phosphors and optoelectronic applications.

Compliance with ethical standards

Disclosure of conflict of interest

The author declare that they have no known competing financial interest or personal relationships that could have appeared to influence the work reported in this paper. The authors received no financial support for the research, authorship, and/or publication of this article. The authors have reviewed and approved this disclosure statement and agree to its inclusion in the research paper.

References

[1] Nazarov M. Luminescent materials and applications. Mater. Sci. Chem. 2016;6:41-74.

[2] Tiwari A, Dhoble SJ. Tunable lanthanide/transition metal ion-doped novel phosphors for possible application in w-LEDs: a review. Luminescence. 2020 Feb;35(1):4-33.

[3] Reddy L. A review of the efficiency of white light (or other) emissions in singly and co-doped Dy3+ ions in different host (phosphate, silicate, aluminate) materials. Journal of Fluorescence. 2023 Nov;33(6):2181-92.

[4] Ugemuge N, Parauha YR, Dhoble SJ. Synthesis and luminescence study of silicate-based phosphors for energy-saving light-emitting diodes. InEnergy materials 2021 Jan 1 (pp. 445-480). Elsevier.

[5] Foka KE. Synthesis and characterization of long afterglow phosphors (SrAl2O4: Ce^3+, SrAl2O4: Tb^3+, CaAlxOy: Tb^3+, Y3Al5O12: Eu^3+) using solution combustion method (Doctoral dissertation, University of the Free State).

[6] Yan Y, Huo H, Zhang H, Zhao T, Wang Q, Zou X, Su C. Preparation and luminescence of Dy3+ doped glass-ceramics containing ZnMoO4. Journal of Non-Crystalline Solids. 2021 Oct 1;569:120990.

[7] Gupta SK, Mohapatra M, Natarajan V, Godbole SV. Photoluminescence Investigations of the Near White Light Emitting Perovskite Ceramic SrZrO 3: Dy 3+ Prepared Via Gel-Combustion Route. International Journal of Applied Ceramic Technology. 2013 Jul;10(4):593-602.

[8] Matsuzawa T, Aoki Y, Takeuchi N, Murayama YJ. A new long phosphorescent phosphor with high brightness, SrAl2 O 4: Eu2+, Dy3+. Journal of the Electrochemical Society. 1996 Aug 1;143(8):2670-3.

[9] Johnson C, Affolter MD, Inkenbrandt P, Mosher C. 3 Minerals. An Introduction to Geology. 2017 Jul 1.

[10] Saito Y, Takao H, Tani T, Nonoyama T, Takatori K, Homma T, Nagaya T, Nakamura M. Lead-free piezoceramics. Nature. 2004 Nov 4;432(7013):84-7.

[11] Aynaya-Cahui SC, Cano NF, Lopez-Gonzales AH, Rao TG, Gomes MB, Rocca RR, Chubaci JF, Watanabe S, Ayala-Arenas JS. Thermoluminescence and electron paramagnetic resonance correlation studies in lithium silicate phosphor. Solid State Sciences. 2022 Jan 1;123:106777.

[12] Wani MA, Belekar RM, Athawale SA, Wankhede YB, Muley GG, Kakde AS, Raghuvanshi MR. Energy transfer mechanism of Eu2+, Mn2+ Doped lithium aluminate phosphor: Synthesis, Hirshfeld surface analysis and optical study. Materials Chemistry and Physics. 2022 Dec 1;292:126796.

[13] Kakde AS, Wakde GC, Wani MA, Gaikwad VM, Meshram NS, Lad AB, Rewatkar KG, Belekar RM. Exploration of Ce+ 3 substitution on electron density distribution, optical, and magnetic properties of Ni-Co-Zn spinel nano-ferrites. Journal of Sol-Gel Science and Technology. 2023 Aug;107(2):401-16.

[14] Wang F, Wang W, Zhang L, Zheng J, Jin Y, Zhang J. Luminescence properties and its red shift of blue-emitting phosphor Na 3 YSi 3 O 9: Ce 3+ for UV LED. Rsc Advances. 2017;7(44):27422-30.

[15] Varma A, Mukasyan AS, Rogachev AS, Manukyan KV. Solution combustion synthesis of nanoscale materials. Chemical reviews. 2016 Dec 14;116(23):14493-586.

[16] Tang W, Guo Q, Su K, Liu H, Zhang Y, Mei L, Liao L. Structure and photoluminescence properties of Dy3+ doped phosphor with whitlockite structure. Materials. 2022 Mar 15;15(6):2177.

[17] Scientific TF. Band Gap Analysis Through UV-Visible Spectroscopy. Thermo Fisher Scientific: Waltham, MA, USA. 2023.

[18] Gupta SK, Saikh Z, Sudarshan K, Bhattacharyya K, Kadam RM. Doped lanthanum cerate pyrochlore for multicolor luminescent phosphor: Decisive role of energy transfer and defects. Journal of Luminescence. 2021 Aug 1;236:118072.

[19] Wang Y, Ding J, Wang Y, Zhou X, Cao Y, Ma B, Li J, Wang X, Seto T, Zhao Z. Structural design of new Ce 3+/Eu 2+-doped or co-doped phosphors with excellent thermal stabilities for WLEDs. Journal of Materials Chemistry C. 2019;7(7):1792-820.